JOURNAL OF GUIDANCE, CONTROL, AND DYNAMICS
Vol. 20, No. 2, March–April 1997

Optimal Earth–Moon Trajectories Using Nuclear Electric Propulsion

Craig A. Kluever*
University of Missouri–Columbia/Kansas City, Kansas City, Missouri 64110-2499
and
Bion L. Pierson†
Iowa State University, Ames, Iowa 50011-3231

Minimum-fuel, two-dimensional and three-dimensional, Earth–moon trajectories are obtained for a nuclear electric propulsion spacecraft. The initial state is a circular low Earth parking orbit and the terminal state is a circular low lunar parking orbit. For the three-dimensional problem, the lunar orbit is inclined 90 deg to the Earth–moon plane. The trajectory has a fixed thrust-coast-thrust engine sequence and is governed by the classical restricted three-body problem dynamic model. An analytical expression for quasicircular low-thrust transfers is used to approximate and replace the hundreds of initial and final orbits about the Earth and moon. A costate-control transformation is also utilized to enhance convergence to the optimal solution. Numerical results are presented for the optimal Earth–moon trajectories.

Nomenclature

a_T	= thrust acceleration magnitude
D	= constant separation distance between the Earth and moon
$\boldsymbol{f}$	= right-hand-side vector of the state equation $\dot{\boldsymbol{x}} = \boldsymbol{f}(\boldsymbol{x}, u, v, t)$
H	= Hamiltonian function
I_{sp}	= specific impulse
i	= specified inclination with respect to the Earth–moon plane
m	= vehicle mass
m_0, m_f	= initial and final spacecraft mass for a quasicircular Edelbaum transfer
$\dot{m}$	= propellant mass flow rate
n	= constant product of ω and r_3
r	= radial distance to the spacecraft
T	= thrust magnitude
t	= time
t_c	= flight time for the powered lunar capture
t_e	= flight time for the powered Earth escape
t_f	= final time
u	= thrust steering angle measured positive above the local horizontal plane to the projection of the thrust vector onto the local longitude-radial direction vertical plane
$\dot{u}, \dot{v}$	= thrust steering angle time rates
V_1, V_2	= initial and final circular orbit speeds for a quasicircular Edelbaum transfer
v	= thrust steering angle measured positive above the local vertical plane to the thrust vector (first or fourth quadrant only)
v_{cir}	= circular orbital speed for the desired final radial distance r_{LLO}
v_r, v_θ, v_ϕ	= orthogonal spherical coordinate velocity components
v_{θ_I}, v_{ϕ_I}	= inertial velocity components along the local longitude and latitude planes, respectively, with respect to a fixed, moon-centered, spherical frame
$\boldsymbol{x}$	= six-element state vector
Δi	= plane change in degrees for a quasicircular Edelbaum transfer
ΔV	= velocity increment for a quasicircular Edelbaum transfer
θ	= spherical coordinate longitude angle measured in the Earth–moon plane counter-clockwise from the Earth–moon line to the projection of the spacecraft position vector
$\boldsymbol{\lambda}$	= costate vector $[\lambda_r \ \ \lambda_{v_r} \ \ \lambda_{v_\theta} \ \ \lambda_{v_\phi} \ \ \lambda_\theta \ \ \lambda_\phi]^T$
$\boldsymbol{\lambda}_v$	= velocity costate vector $[\lambda_{v_r} \ \ \lambda_{v_\theta} \ \ \lambda_{v_\phi}]^T$
μ_e, μ_m	= gravitational parameters for the Earth and moon, respectively
$\boldsymbol{\nu}$	= terminal state constraint multiplier vector
τ	= initial time for powered lunar capture, $t_f - t_c$
Φ	= Mayer performance index
ϕ	= spherical coordinate latitude angle measured from the Earth–moon plane projection of the spacecraft position vector to the position vector, positive if the position vector lies above the Earth–moon plane
$\boldsymbol{\Psi}$	= terminal state constraint residual vector
ψ	= heading angle measured from the local latitude line (local easterly direction) to the projection of the velocity vector onto the horizontal plane
ω	= constant angular rotation rate of the Earth–moon system

Subscripts

1	= Earth-escape spiral phase
2	= translunar coast phase
3	= moon-capture spiral phase

Superscript

*	= optimal

Introduction

SPACECRAFT propelled by low-thrust engines are capable of delivering a greater payload fraction compared to spacecraft using conventional chemical propulsion systems.[1,2] The use of electric propulsion for Earth–moon transfers has been a popular topic for research.[3–10] References 3 and 4 present low-thrust lunar

Presented as Paper 95-399 at the AAS/AIAA Astrodynamics Specialist Conference, Halifax, NS, Canada, Aug. 14–17, 1995; received Aug. 25, 1995; revision received Oct. 28, 1996; accepted for publication Nov. 6, 1996.

*Assistant Professor, Mechanical and Aerospace Engineering. Member AIAA.

†Professor, Department of Aerospace Engineering and Engineering Mechanics. Associate Fellow AIAA.

transfers using power-limited spacecraft whereas Refs. 5–10 employ constant-thrust electric propulsion systems. In addition, nuclear electric propulsion (NEP) has been identified as a potential propulsion mode for large-scale spacecraft with fairly high-power requirements.[10–14]

This paper extends our earlier work on optimal two-dimensional and three-dimensional Earth–moon transfers with a moderate thrust-to-weight (T/W) ratio of $3(10^{-3})$ (Refs. 5 and 7). The NEP spacecraft T/W ratio treated is more than an order of magnitude lower than $3(10^{-3})$, and consequently the NEP transfer involves a greatly increased transfer time with numerous near-circular orbits about the Earth and moon. Furthermore, a costate-control transformation is included in our treatment of the optimal controls, and unlike our previous work,[10] the Edelbaum approximation is applied here in a full three-dimensional setting. We present solutions to a minimum-fuel transfer problem between a circular, low Earth orbit (LEO) and a circular, low lunar orbit (LLO). Both an optimal planar transfer and an optimal three-dimensional transfer to polar LLO are obtained. The restricted (circular) three-body problem dynamic model is used to generate the optimal Earth–moon trajectory. The trajectory is assumed to consist of a continuous-thrust Earth-escape spiral, followed by a translunar coast arc, and finally a continuous-thrust moon-capture spiral.

Trajectory Optimization

Dynamics

Classical restricted three-body problem equations of motion[15,16] are used for the Earth–moon trajectories. The three-dimensional dynamic equations are expressed in rotating spherical coordinates, with the Earth–moon plane as the primary plane. Thus, the six elements of the state vector $\boldsymbol{x}$ consist of the three position variables, r, θ, and ϕ, plus the three velocity components, v_r, v_θ, and v_ϕ. There is no mass rate equation since the assumption of a constant mass flow rate results in a linear mass time history during each thrusting segment. Earth-centered spherical coordinates are used for both the thrusting Earth-escape phase and the translunar coast phase. However, the equations of motion for the thrusting moon-capture phase are referred to a moon-centered spherical coordinate frame. Two control functions, the thrust steering angles $u(t)$ and $v(t)$, define the orientation of the thrust vector during the powered escape and capture phases. The specific equations of motion used here may be found in Ref. 7. Although spherical coordinates are exclusively used in this analysis, the use of other coordinate systems could prove beneficial. All differential equations of motion are numerically integrated using the variable-step Adams–Moulton routine DIVPAG from the International Mathematics and Statistics Library[17] with a prescribed truncation error of 10^{-7}.

Vehicle Model

The spacecraft characteristics adopted here represent an ion NEP lunar cargo vehicle[13,14] with a total initial mass in LEO m_{LEO} of 123,000 kg. The constant input power is 5000 kW, and the constant specific impulse I_{sp} is 5000 s. Thruster efficiency is fixed at 75%, and therefore thrust magnitude T and propellant mass flow rate $\dot{m}$ are both constant at 152.9 N and 269.3 kg/day, respectively. The corresponding initial T/W ratio is $1.3(10^{-4})$ and is less than 1/20 of the T/W ratio utilized in Refs. 5 and 7. For our analysis, the low-thrust engines are assumed to operate without a transient start-up or tail-off period, and therefore T and $\dot{m}$ are considered to be at their respective constant values during powered flight or at zero during the coast phase.

Problem Statement

The optimal control problem treated here is a free end-time problem and involves both control functions and control parameters. In the three-dimensional setting, the problem can be stated formally as follows.

Find the initial longitude angle $\theta_1(0)$, the thrust steering time histories $u_1(t)$ and $v_1(t)$, $0 \le t \le t_e$, and $u_3(t)$ and $v_3(t)$, $\tau \le t \le t_f$, the powered flight durations t_e and t_c, and the final time t_f that minimize

$$J = t_e + t_c = \Phi[t_e, t_c, \boldsymbol{x}(t_f), t_f] \tag{1}$$

subject to the three-dimensional restricted three-body equations of motion with the boundary conditions at $t = 0$

$$r_1(0) = r_{\text{LEO}} \tag{2}$$

$$v_{r_1}(0) = 0 \tag{3}$$

$$v_{\theta_1}(0) = \sqrt{(\mu_e / r_{\text{LEO}})} - \omega r_{\text{LEO}} \tag{4}$$

$$v_{\phi_1}(0) = 0 \tag{5}$$

$$\phi_1(0) = 0 \tag{6}$$

the boundary conditions at $t = t_e$

$$\boldsymbol{x}_2(t_e) = \boldsymbol{x}_1(t_e) \tag{7}$$

the boundary conditions at $t = \tau$

$$\boldsymbol{x}_3(\tau) = \boldsymbol{g}[\boldsymbol{x}_2(\tau), D] \tag{8}$$

and the terminal state constraints

$$\boldsymbol{\Psi}[\boldsymbol{x}_3(t_f), t_f] = \begin{pmatrix} r_3(t_f) - r_{\text{LLO}} \\ v_{r_3}(t_f) \\ v_{\theta_I}^2(t_f) + v_{\phi_I}^2(t_f) - v_{\text{cir}}^2 \\ v_{\theta_I}(t_f)\cos\phi_3(t_f) - v_{\text{cir}}\cos i \end{pmatrix} = \begin{pmatrix} 0 \\ 0 \\ 0 \\ 0 \end{pmatrix} \tag{9}$$

The initial state conditions [Eqs. (2–6)] define an initial 407-km altitude, low Earth circular orbit with zero inclination. Since inclination is measured from the Earth–moon plane, the initial orbit is contained in that plane. Equation (7) represents the required state matching conditions at the end of the Earth-escape phase ($t = t_e$) between the powered and coasting trajectory segments. Equation (8) enforces the required state matching conditions between the Earth-centered coasting arc and the moon-centered powered capture trajectory. The functional relationship $\boldsymbol{g}[\boldsymbol{x}_2(\tau), D]$ represents the required coordinate transformation between the two rotating frames and is detailed in Appendix A of Ref. 7.

The four terminal state constraints [Eq. (9)] define a circular 100-km altitude LLO with a specified inclination i with respect to the Earth–moon plane. The terminal state constraints are expressed in the moon-centered, rotating, spherical coordinate system. The first three terminal state constraints specify a low lunar circular orbit. The fourth state constraint ensures termination in an orbit with the desired inclination. Utilizing the relationship between velocities in a fixed reference frame and a rotating reference frame, we obtain the inertial velocity components

$$v_{\theta_I} = v_{\theta_3} + \omega r_3 \cos\phi_3 \tag{10}$$

$$v_{\phi_I} = v_{\phi_3} \tag{11}$$

Because ω is a constant for the restricted three-body problem and the final radius $r_3(t_f)$ is constrained, the product ωr_3 is defined as a constant n. Therefore, the last two terminal state constraints in Eq. (9) are rewritten in terms of velocity components in the rotating frame:

$$\Psi_3 = v_{\theta_3}^2(t_f) + n^2\cos^2\phi_3(t_f) + 2v_{\theta_3}(t_f)n\cos\phi_3(t_f) + v_{\phi_3}^2(t_f) - v_{\text{cir}}^2 = 0 \tag{12}$$

$$\Psi_4 = v_{\theta_3}(t_f)\cos\phi_3(t_f) + n\cos^2\phi_3(t_f) - v_{\text{cir}}\cos i = 0 \tag{13}$$

Although the third terminal state constraint in Eq. (9) [Eq. (12)] involves nonlinear terms, it provides a compact representation of the requirement for the magnitude of the final velocity vector to match the circular orbital speed in LLO.

Solution Method

Three-Stage Approach

The nonlinear three-body dynamics, coupled with the strict requirement for the transfer to terminate in a low circular lunar orbit under the control of a low-thrust engine, results in an optimization solution process that is extremely sensitive to initial guesses for spacecraft control. Therefore, the prospect of obtaining the minimum-fuel LEO–LLO trajectory by solving numerically a single optimization problem seems very remote. Our previous paper[5] presented a systematic three-stage approach for obtaining the minimum-fuel Earth–moon trajectory. Tang and Conway[18] have recently applied a similar systematic procedure for obtaining minimum-fuel interplanetary trajectories. Our hierarchal approach is briefly outlined as follows.

1) The first stage involves computing several optimal low-thrust Earth-escape and moon-capture trajectories that maximize total energy at the end/start of a fixed-time transfer based on two-body dynamics.

2) In the second stage, we compute an all-coasting, suboptimal, minimum-fuel trajectory between boundary conditions provided by curve-fitting the maximum-energy escape/capture spirals obtained from the first stage. Restricted three-body dynamics without thrusting terms are used here.

3) Finally, the complete minimum-fuel, LEO–LLO, trajectory problem with a thrust-coast-thrust engine sequence is solved. A hybrid direct/indirect method is used to solve this optimal control problem.

The associated nonlinear programming problems are solved using sequential quadratic programming (SQP), which is a constrained parameter optimization method.[19] The SQP algorithm used here is the IMSL routine DNCONF.[17] For the first-stage problem, the corresponding two-point boundary value problem (2PBVP) from optimal control theory[20] is solved via SQP with the initial costate variables as SQP parameters and the transversality conditions enforced through SQP equality constraints. This maximum-energy Earth-escape problem has also recently been addressed by Herman and Conway.[21] The second-stage problem converges very rapidly due to the small number of SQP problem variables and the replacement of the long-duration escape/capture spirals with curve-fit boundary conditions. A parameterization of the thrust direction angles $u(t)$ and $v(t)$, as outlined in the following section, is used to solve the third-stage problem.

Hybrid Direct/Indirect Method

In general, an optimal control problem may be solved using either a direct or indirect method. An indirect method involves solving the corresponding 2PBVP, which is usually an extremely difficult task except in the case of a simple dynamic system. A direct method utilizes a parameterization of the control and attempts to directly reduce the performance index value at each iteration. Because our minimum-fuel problem involves sensitive system dynamics and a dual coordinate frame, a direct optimization method is used here. The optimal control problem is replaced with an approximate nonlinear programming problem with the continuous control history replaced with a finite number of parameters. A typical approach to parameterizing the control is to utilize linear or cubic spline interpolation through a fixed number of control points. For the long-duration spiral trajectories, this technique would require a very large number of control points for sufficient accuracy. A more efficient and accurate technique is to utilize the necessary conditions from optimal control theory[20] to parameterize the control angle time histories. As a result, the optimal thrust steering angles $u^*(t)$ and $v^*(t)$ are parameterized by the costate differential equations. This parameterization feature utilizes some important aspects of an indirect approach, and therefore this method is termed a hybrid direct/indirect optimization approach.

Necessary Conditions from Optimal Control Theory

The costate equations and transversality conditions are used to define the steering angle time histories. The general form of the costate differential equations is derived for the Earth-centered, rotating, spherical frame, and hence subscripts are not employed.

The Hamiltonian in the Earth-centered, rotating, spherical coordinate frame is

$$H = \boldsymbol{\lambda}^T \boldsymbol{f} \tag{14}$$

The costate differential equations are

$$\dot{\boldsymbol{\lambda}} = -\left(\frac{\partial H}{\partial \boldsymbol{x}}\right)^T \tag{15}$$

The transversality conditions for the moon-centered costate system define the terminal costate values in the inclined LLO. The transversality conditions are obtained from Eqs. (1) and (9):

$$\boldsymbol{\lambda}(t_f) = \left(\left.\frac{\partial \Phi}{\partial \boldsymbol{x}}\right|_{t=t_f} + \boldsymbol{\nu}^T \left.\frac{\partial \Psi}{\partial \boldsymbol{x}}\right|_{t=t_f}\right)^T \tag{16}$$

Application of the stationarity condition yields

$$\frac{\partial H}{\partial u} = 0 = \lambda_{v_r} a_T \cos u \cos v - \lambda_{v_\theta} a_T \sin u \cos v \tag{17}$$

$$\frac{\partial H}{\partial v} = 0 = -\lambda_{v_r} a_T \sin u \sin v - \lambda_{v_\theta} a_T \cos u \sin v + \lambda_{v_\phi} a_T \cos v \tag{18}$$

The resulting direction cosines for the thrust acceleration vector components as required in the equations of motion are

$$\sin u \cos v = -\lambda_{v_r} / \|\boldsymbol{\lambda}_v\| \tag{19}$$

$$\cos u \cos v = -\lambda_{v_\theta} / \|\boldsymbol{\lambda}_v\| \tag{20}$$

$$\sin v = -\lambda_{v_\phi} / \|\boldsymbol{\lambda}_v\| \tag{21}$$

where $\|\boldsymbol{\lambda}_v\| = (\lambda_{v_r}^2 + \lambda_{v_\theta}^2 + \lambda_{v_\phi}^2)^{1/2}$. The correct signs for these direction cosines are obtained by applying the strengthened Legendre–Clebsch condition. A detailed derivation of the costate differential equations, transversality conditions, and stationarity condition is given in Ref. 7.

Edelbaum Approximation for Quasicircular Transfer

The three-stage procedure described was initially attempted for the minimum-fuel two-dimensional transfer problem. The maximum-energy escape/capture spirals and suboptimal coasting trajectory between curve-fit boundaries were obtained in a straightforward fashion for the NEP spacecraft. The complete LEO–LLO transfer was attempted by dividing the trajectory into two segments and numerically integrating the powered Earth-escape spiral and coast arc forward in time from LEO and the moon-capture spiral backwards in time from LLO to a common match point near the lunar sphere of influence (SOI). This matching method has previously been demonstrated to diminish the sensitivities related to the terminal state constraints at circular LLO.[5] However, the minimum-fuel LEO–LLO trajectory problem did not converge due to the extreme number of nearly circular orbits about the Earth and moon. The Earth-escape and moon-capture spirals required about 267 and 37 revolutions about each respective primary body. Because the thrust-direction angle is governed by the sensitive costate system, very small perturbations in the initial guesses for the costates produce extremely different trajectories. In addition, the hundreds of tight, low-altitude, nearly circular orbits require thousands of integration steps and, therefore, greatly increase the computational cost of the problem.

To improve convergence properties and reduce the computational load, the minimum-fuel transfer for the NEP vehicle is now solved from a geosynchronous altitude, circular, Earth orbit (GEO) to a high-altitude, circular, lunar orbit (HLO). Choosing these boundary conditions eliminates hundreds of nearly circular orbits about the Earth and moon from the complete simulation. An auxiliary maximum-energy Earth-escape trajectory to GEO altitude resulted in a final radial velocity of 0.04 km/s and a final eccentricity of 0.01. Thus, this portion of the optimal Earth-escape spiral involves very nearly circular orbits. The HLO altitude is chosen by observing that

the radial velocity time history for an auxiliary maximum-energy moon-capture trajectory remains very small until the spiral time from LLO is about four days. After four days and 28 revolutions about the moon in backward-in-time spiraling from LLO, the radial velocity is −0.02 km/s and the altitude above the moon is 2038 km. Together, the initialization and termination in higher circular orbits removes over 44.6 days of near-circular spiraling and over 289 revolutions about the Earth and moon.

The fuel consumed during these slowly opening, near-circular, spiral trajectories from LEO to GEO and from LLO to 2038-km-altitude HLO is approximated by analytical equations developed by Edelbaum[22] for minimum-fuel, low-thrust, transfer problems between inclined circular orbits. Edelbaum's expression for a low-thrust circle-to-circle transfer with plane change is simply

$$m_f/m_0 = \exp(-\Delta V/gI_{\text{sp}}) \tag{22}$$

The velocity increment ΔV includes the velocity required for a plane change. Edelbaum's expression for ΔV is

$$\Delta V^2 = V_1^2 + V_2^2 - 2V_1V_2\cos(\pi\,\Delta i/2) \tag{23}$$

Therefore, the spacecraft mass in GEO is

$$m_{\text{GEO}} = m_{\text{LEO}}\exp(-\Delta V_e/gI_{\text{sp}}) \tag{24}$$

where ΔV_e is the velocity increment computed from Eq. (23) for the LEO–GEO transfer. The corresponding LEO–GEO quasicircular transfer time Δt_{QC1} is

$$\Delta t_{QC1} = \frac{m_{\text{LEO}} - m_{\text{GEO}}}{\dot{m}} \tag{25}$$

Spacecraft mass at HLO m_{HLO} and HLO–LLO quasicircular transfer time Δt_{QC2} are computed in a similar fashion. These expressions can be used to compute the fuel mass and time required to perform the quasicircular transfers with plane changes from LEO to GEO and from HLO to LLO. The orientations of GEO and HLO are determined by specifying the longitude angle θ, the latitude ϕ, and the heading angle ψ. Both latitude and heading are between ±90 deg. The inclination i of GEO (or HLO) is then computed from

$$\cos i = \cos\phi\cos\psi \tag{26}$$

Because only posigrade orbits are considered, i is between zero and 90 deg. The initial and final velocity components with respect to an inertial frame for the inclined GEO and HLO are

$$v_r = 0 \tag{27}$$

$$v_\theta = v_{\text{cir}}\cos\psi \tag{28}$$

$$v_\phi = v_{\text{cir}}\sin\psi \tag{29}$$

Costate-Control Transformation

The state matching conditions between the forward-in-time and backward-in-time trajectory segments are extremely sensitive to changes in the initial costate values, and this hinders the convergence of the SQP problem. The convergence properties for the minimum-fuel GEO–HLO problem are improved by introducing a costate-control transformation.[23] Reference 23 presents the costate-control transformation for a planar problem; we have extended the transformation to the three-dimensional problem. Instead of guessing and iterating on the unknown costate values at GEO and HLO, the values for the initial thrust steering angles and steering rates (u, $\dot{u}$, v, and $\dot{v}$) are the SQP design variables. Because costate values are nonlinearly related to u, $\dot{u}$, v, and $\dot{v}$, the initial costate values can be computed. Choosing the initial control state as design variables has more physical meaning than selecting costate values as design variables. Details of the three-dimensional costate-control transformation are presented in the Appendix.

The use of the Edelbaum quasicircular approximation and the costate-control transformation results in a different nonlinear programming problem than for the LEO–LLO problem. To summarize this change, we can list the specific design variables used here for the GEO–HLO problem, including the Edelbaum approximation and the costate-control transformation. For the three-dimensional problem, the SQP formulation has 17 design variables: the initial and final longitude, latitude, and heading angles in GEO and HLO, the initial and final thrust steering angles and steering rates in GEO and HLO, the durations of the powered escape and capture spirals, and the duration of the coast arc. The orbit inclination and velocity components v_θ and v_ϕ in GEO and HLO are computed using the latitude and heading angles and the respective circular orbit velocities. The SQP problem has six equality constraints, which require position and velocity matching near the SOI. For the simpler two-dimensional problem, the SQP formulation has nine design variables and four equality constraints.

Note that our parameterization of the controls leads to a relatively small total number of design variables but does not necessarily greatly reduce the inherent sensitivity in the numerical solution process. Other direct optimization techniques (such as collocation methods) may improve robustness properties at the expense of greatly expanding the design parameter space.

Numerical Results

Two-Dimensional Transfers

The minimum-fuel, two-dimensional, GEO–HLO transfer is obtained first using the hybrid direct/indirect method with the costate-control transformation. The resulting optimal spacecraft mass in the HLO after numerical integration of the three-body equations of motion from GEO is 106,290 kg. Edelbaum's analytical method is then used to compute the final spacecraft mass in LLO, and the result is 105,225 kg. The minimum-fuel trajectory for the NEP vehicle results in a final-mass-to-initial-mass ratio of 0.8555.

It would be desirable to have a direct comparison between optimal trajectories with and without the Edelbaum approximation. But that is not possible because we were not able to obtain a solution to the full LEO–LLO transfer problem; that, of course, is the primary motivation for adopting the Edelbaum approximation. However, we can compare with the suboptimal (stage 2) all-coast solution to the LEO–LLO problem. That suboptimal solution delivered 105,217 kg to LLO for a final-mass-to-initial-mass ratio of 0.8554. Therefore, very little improvement in performance is made between the suboptimal solution and the complete minimum-fuel GEO–HLO solution with Edelbaum's analytical approximations.

For the full optimal transfer, the NEP vehicle completes about 261 revolutions about the Earth in 40.64 days during the Edelbaum approximation for the LEO–GEO quasicircular transfer. The optimal numerically simulated trajectory completes six revolutions about the Earth during a 14.55 day escape spiral from circular GEO to the start of the translunar coast arc. The NEP vehicle coasts for 6.76 days before spiraling for 6.56 days and nine revolutions during the moon capture terminating at HLO. Edelbaum's analytical method approximates the quasicircular transfer from HLO to LLO at 3.94 days. The trip time for the numerically simulated GEO–HLO transfer is 27.87 days, which is slightly greater than one lunar orbit period. The total trip time for the LEO–LLO transfer is 72.44 days. The minimum-fuel GEO–HLO trajectory is shown in the Earth-centered, rotating frame in Fig. 1 and in an inertial Earth-centered frame in Fig. 2. The inertial plot indicates the moon's position at the start of the escape spiral from GEO and at the end of the lunar capture into HLO.

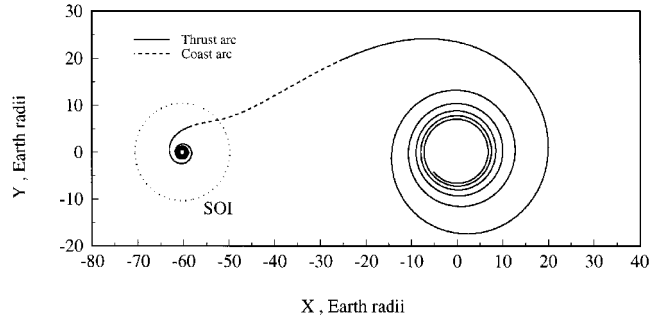

Fig. 1 Optimal two-dimensional trajectory for NEP vehicle: rotating coordinates.

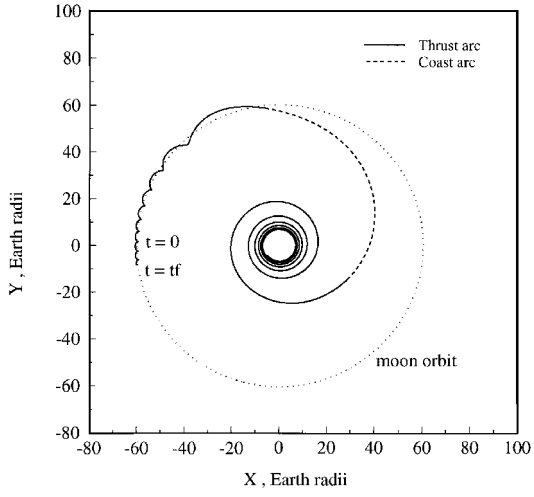

Fig. 2 Optimal two-dimensional trajectory for NEP vehicle: inertial coordinates.

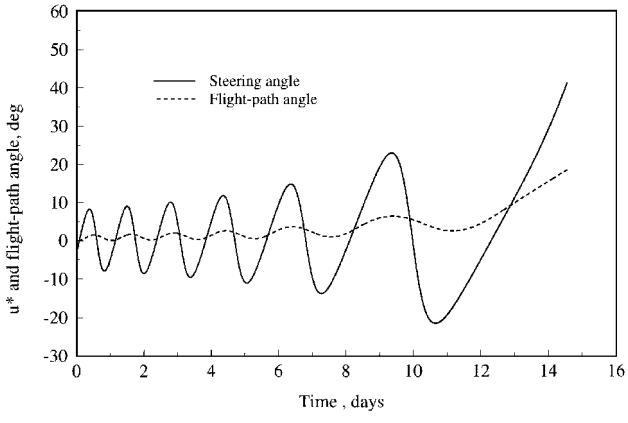

Fig. 3 Optimal steering and flight-path angles: Earth escape.

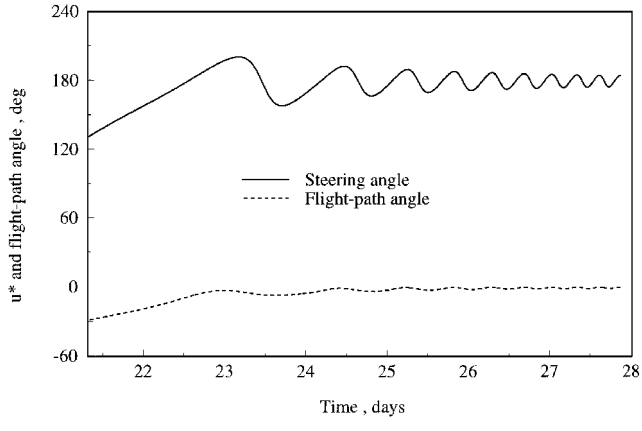

Fig. 4 Optimal steering and flight-path angles: moon capture.

There is a slight overlap in the moon orbit since the GEO–HLO trip time slightly exceeds the period of the moon's orbit about the Earth–moon center of mass. The optimal thrust steering angle time histories along with the flight-path angles for the Earth-escape and moon-capture spirals are shown in Figs. 3 and 4.

Three-Dimensional Transfer to Polar Lunar Orbit

The minimum-fuel three-dimensional trajectory to a polar lunar orbit is obtained next. For the minimum-fuel three-dimensional trajectory, the initial LEO has zero inclination and the final LLO is a polar orbit with a 90-deg inclination with respect to the Earth–moon plane. The circular boundary orbits for the numerical integration, GEO and HLO, may be at any inclination because the optimization process is free to allocate the 90-deg plane change among the LEO–GEO, GEO–HLO, and HLO–LLO segments. Edelbaum's analytical expressions are used to compute the fuel mass and time duration required to perform the quasicircular transfers with plane changes from LEO to GEO and from HLO to polar LLO.

Again, the hybrid direct/indirect method is used to solve the minimum-fuel three-dimensional trajectory for the NEP vehicle. The two-dimensional minimum-fuel solution provides the initial guess. Therefore, the initial latitude ϕ, heading ψ, inclination i, steering angle v, and steering rate $\dot{v}$ are all zero in both GEO and HLO for the initial guess and the zeroth iteration simply results in the optimal planar transfer between GEO and HLO. Because the initial guess is from the two-dimensional solution, the Edelbaum quasicircular transfer from LEO to GEO is planar and the quasicircular transfer from HLO to polar LLO performs the entire 90-deg plane change. The initial and final inclination requirements are maintained by the Edelbaum approximations. The respective plane change requirements from the analytical quasicircular transfers influence the SQP performance index, total powered flight time.

The convergence history of the three-dimensional problem is presented in Table 1. Because the latitude and heading in GEO and HLO are SQP design variables, the inclinations of GEO and HLO are free. The table shows how the inclinations of GEO and HLO change as the SQP problem converges to a solution in 158 iterations. In the fourth column, the plane change performed by the Edelbaum approximation for the transfer from HLO to polar LLO is presented. The zeroth iteration is the two-dimensional solution, and the poor performance as shown by the final mass in LLO (column five) is due to the complete 90-deg plane change performed by the Edelbaum approximation. As the SQP solution progresses, the inclinations of GEO and HLO increase, and the resulting mass in polar LLO increases. The optimal spacecraft mass in polar LLO is 104,888 kg, which is only 337 kg less than the final mass from the optimal two-dimensional NEP trajectory. Therefore, the optimal three-dimensional NEP trajectory requires only 1.9% more fuel than the minimum-fuel two-dimensional trajectory.

The optimal three-dimensional trajectory for the NEP vehicle is shown in the Earth-centered, rotating frame in Figs. 5 and 6. Figure 5 presents the projection of the three-dimensional trajectory onto the Earth–moon plane, and Fig. 6 shows the projection onto the vertical plane containing the Earth–moon line. The optimal trajectory completes six revolutions about the Earth during a 15.18-day escape spiral from GEO. At the end of the Earth-escape spiral, the orbit is inclined 2.8 deg with respect to the Earth. As indicated in Fig. 6, the spacecraft is lofted above the Earth–moon plane during the 4.63-day coast arc. In Fig. 6, the vertical axis is distorted to emphasize the out-of-plane motion. The spacecraft reaches a peak of over 6.9 Earth radii above the Earth–moon plane during the coast arc. Shortly after the vertical peak of the coast trajectory, the spacecraft coasts toward the Earth–moon plane and the moon-capture spiral is initiated. At this point, the spacecraft is above the moon's orbit with an

Table 1 Convergence history for minimum-fuel three-dimensional NEP trajectory

Iteration	i_{GEO}, deg	i_{HLO}, deg	Δi, HLO–LLO, deg	m_{LLO}, kg
0	0.00	0.00	90.0	100,756.1
10	4.27	14.55	75.5	101,074.9
20	5.07	19.59	70.4	101,244.2
30	7.98	31.51	58.5	101,619.5
40	13.66	66.82	23.2	103,235.3
50	12.97	79.91	10.1	104,171.6
60	12.32	82.30	7.7	104,307.8
70	11.99	82.79	7.2	104,349.4
80	8.73	84.79	5.2	104,672.0
90	6.46	88.09	1.9	104,822.9
100	5.48	87.94	2.1	104,859.5
110	4.55	87.80	2.2	104,872.9
120	4.16	88.47	1.5	104,879.4
130	4.15	88.52	1.5	104,880.0
140	3.48	89.34	0.7	104,886.3
150	3.51	89.29	0.7	104,887.7
158	3.51	89.29	0.7	104,887.8

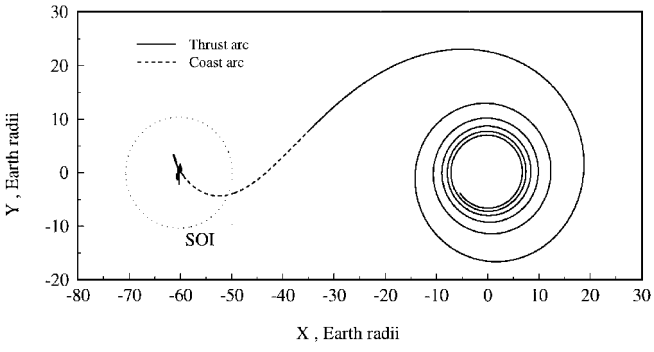

Fig. 5 Optimal three-dimensional trajectory: x–y plane in rotating frame.

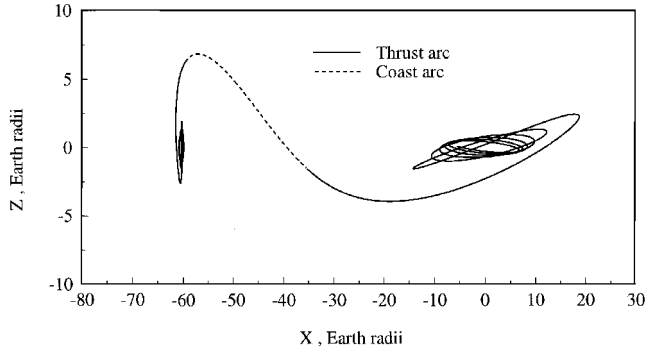

Fig. 6 Optimal three-dimensional trajectory: x–z plane in rotating frame.

inclination of 86.5 deg. The moon-capture spiral lasts for 6.98 days and completes the 2.8-deg plane change to the 89.3-deg inclined circular HLO. The quasicircular transfer from HLO to polar LLO is approximated by Edelbaum's analytical equations.

Conclusions

This analysis allows us to treat a realistic nuclear electric vehicle model with its relatively low thrust-to-weight ratio. Both the Edelbaum approximation and the costate-control transformation proved to be essential in obtaining numerical solutions for the initial thrust-to-weight ratio of $1.3(10^{-4})$ treated here. The Edelbaum approximation is particularly useful for the three-dimensional case since it allows a plane change capability for the quasicircular segments.

For the optimal two-dimensional trajectories, the performance difference between 1) the complete GEO to HLO solution with the Edelbaum approximation and 2) the suboptimal, all-coast, LEO to LLO solution is very nearly negligible. But of course, only the former solution provides a definition of the optimal translunar steering.

For the three-dimensional case, the large majority of the 90-deg plane change occurs during the GEO to HLO transfer. Thus, the quasicircular spiral segments at each end of the optimal transfer are nearly planar.

The optimal three-dimensional transfer to polar LLO requires a fuel penalty of less than 2% compared to the optimal two-dimensional transfer. The orbit plane at the start of the powered lunar capture spiral is nearly normal to the Earth–moon line. Our previous experience suggests that this fuel penalty will increase significantly if the target polar lunar orbit plane is constrained to be more closely aligned with the Earth–moon line.

Appendix: Three-Dimensional Costate-Control Transformation

The nonlinear relationships between the state of the controls for the three-dimensional transfer (u, $\dot{u}$; v, $\dot{v}$) and the costates are derived in this section. The thrust acceleration direction cosines are again given by

$$\sin u \cos v = -\lambda_{v_r}/\|\boldsymbol{\lambda}_v\| \tag{A1}$$

$$\cos u \cos v = -\lambda_{v_\theta}/\|\boldsymbol{\lambda}_v\| \tag{A2}$$

$$\sin v = -\lambda_{v_\phi}/\|\boldsymbol{\lambda}_v\| \tag{A3}$$

The norm $\|\boldsymbol{\lambda}_v\|$ can be scaled and set equal to unity. Therefore, given the initial steering angles u and v, the initial velocity costates λ_{v_r}, λ_{v_θ}, and λ_{v_ϕ} can be calculated from Eqs. (A1–A3).

To determine the initial radial position costate λ_r, the first time derivative of the thrust direction angle u from the inverse-tangent steering law is computed:

$$\dot{u} = \frac{\mathrm{d}}{\mathrm{d}t}\left[\tan^{-1}\left(\frac{\lambda_{v_r}}{\lambda_{v_\theta}}\right)\right] = \frac{1}{\sec^2 u}\frac{\lambda_{v_\theta}\dot{\lambda}_{v_r} - \lambda_{v_r}\dot{\lambda}_{v_\theta}}{\lambda_{v_\theta}^2} \tag{A4}$$

The differential costate equations for λ_{v_r} and λ_{v_θ} from Ref. 7 are substituted. Solving for λ_r and noting that at t_0 and t_f both the radial velocity v_r and the longitude angle costate λ_θ are zero, we find that

$$\lambda_r = \frac{1}{\lambda_{v_\theta}}\left[-\dot{u}\left(\lambda_{v_r}^2 + \lambda_{v_\theta}^2\right) + 2\lambda_{v_r}^2\left(\omega\cos\phi + \frac{v_\theta}{r}\right)\right.$$
$$+\lambda_{v_\theta}^2\left(2\omega\cos\phi + \frac{v_\theta}{r}\right) + \lambda_{v_\theta}\lambda_{v_\phi}\frac{v_\phi}{r} + \lambda_{v_r}\lambda_{v_\theta}\frac{v_\phi\tan\phi}{r}$$
$$\left.-2\lambda_{v_r}\lambda_{v_\phi}\left(\omega\sin\phi + \frac{v_\theta\tan\phi}{r}\right)\right]\Bigg|_{t=t_0} \tag{A5}$$

The meridian angle costate λ_ϕ is determined from the first time derivative of the meridian steering angle v. The steering law for v from the optimality condition (18) is

$$v = \tan^{-1}\left(\frac{-\lambda_{v_\phi}}{\left(\lambda_{v_r}^2 + \lambda_{v_\theta}^2\right)^{\frac{1}{2}}}\right) \tag{A6}$$

The first time derivative is

$$\dot{v} = \frac{1}{\sec^2 v}\frac{\left[-\left(\lambda_{v_r}^2 + \lambda_{v_\theta}^2\right)^{\frac{1}{2}}\dot{\lambda}_{v_\phi} + \lambda_{v_\phi}\mathrm{d}/\mathrm{d}t\left(\lambda_{v_r}^2 + \lambda_{v_\theta}^2\right)^{\frac{1}{2}}\right]}{\lambda_{v_r}^2 + \lambda_{v_\theta}^2} \tag{A7}$$

Substituting for $\dot{\lambda}_{v_\phi}$ and $\sec^2 v$ and expanding, we get

$$\dot{v} = \frac{1}{\|\boldsymbol{\lambda}_v\|^2}\left[-\left(\lambda_{v_r}^2 + \lambda_{v_\theta}^2\right)^{\frac{1}{2}}\left[-\lambda_{v_r}\frac{2v_\phi}{r}\right.\right.$$
$$\left.-\lambda_{v_\theta}\left(2\omega\sin\phi + \frac{v_\theta\tan\phi}{r}\right) + \lambda_{v_\phi}\frac{v_r}{r} - \frac{\lambda_\phi}{r}\right]$$
$$\left.+\lambda_{v_\phi}\frac{\lambda_{v_r}\dot{\lambda}_{v_r} + \lambda_{v_\theta}\dot{\lambda}_{v_\theta}}{\left(\lambda_{v_r}^2 + \lambda_{v_\theta}^2\right)^{\frac{1}{2}}}\right] \tag{A8}$$

Because $\dot{\lambda}_{v_r}$ and $\dot{\lambda}_{v_\theta}$ do not explicitly depend on λ_ϕ, the differential equations are not substituted to simplify the expression. The norm $\|\boldsymbol{\lambda}_v\|$ is set to unity and v_r is set to zero. Solving the preceding equation for λ_ϕ yields

$$\lambda_\phi = \frac{\dot{v}r}{\left(\lambda_{v_r}^2 + \lambda_{v_\theta}^2\right)^{\frac{1}{2}}} - 2\lambda_{v_r}v_\phi - \lambda_{v_\theta}r\left(2\omega\sin\phi + \frac{v_\theta\tan\phi}{r}\right)$$
$$-\lambda_{v_\phi}\frac{\lambda_{v_r}\dot{\lambda}_{v_r} + \lambda_{v_\theta}\dot{\lambda}_{v_\theta}}{\lambda_{v_r}^2 + \lambda_{v_\theta}^2} \tag{A9}$$

The expressions substituted for the costate differential equations are the same for the Earth-centered and moon-centered coordinate frames with the states referenced to the respective frames. Because the trajectory terminates in circular orbits, v_r is zero at both ends. Also, as indicated by the transversality conditions, λ_θ is zero in the two terminal circular orbits. Therefore, Eqs. (A5) and (A9) determine the position costates λ_r and λ_ϕ at both ends of the trajectory given the values u, $\dot{u}$, v, and $\dot{v}$ in circular Earth orbit and circular lunar orbit.

Acknowledgments

This research was begun under the NASA Graduate Student Researchers Program and Grant NGT-50637. The authors would especially like to thank John Riehl at the NASA Lewis Research Center for his suggestions and contributions to this research project.

References

[1]Jones, R. M., "Comparison of Potential Electric Propulsion Systems for Orbit Transfer," *Journal of Spacecraft and Rockets*, Vol. 21, No. 1, 1984, pp. 88–95.

[2]Hermel, J., Meese, R. A., Rogers, W. P., Kushida, R. O., Beattie, J. R., and Hyman, J., "Modular, Ion-Propelled, Orbit-Transfer Vehicles," *Journal of Spacecraft and Rockets*, Vol. 25, No. 5, 1988, pp. 368–374.

[3]Golan, O. M., and Breakwell, J. V., "Minimum Fuel Lunar Trajectories for Low-Thrust Power-Limited Spacecraft," AIAA Paper 90-2975, Aug. 1990.

[4]Guelman, M., "Earth-to-Moon Transfer with a Limited Power Engine," *Journal of Guidance, Control, and Dynamics*, Vol. 18, No. 5, 1995, pp. 1133–1138.

[5]Pierson, B. L., and Kluever, C. A., "Three-Stage Approach to Optimal Low-Thrust Earth–Moon Trajectories," *Journal of Guidance, Control, and Dynamics*, Vol. 17, No. 6, 1994, pp. 1275–1282.

[6]Kluever, C. A., and Pierson, B. L., "Optimal Low-Thrust Earth–Moon Transfers Using a Switching Function Structure," *Journal of the Astronautical Sciences*, Vol. 42, No. 3, 1994, pp. 269–283.

[7]Kluever, C. A., and Pierson, B. L., "Optimal Low-Thrust Three-Dimensional Earth–Moon Trajectories," *Journal of Guidance, Control, and Dynamics*, Vol. 18, No. 4, 1995, pp. 830–837.

[8]Enright, P. J., and Conway, B. A., "Discrete Approximations to Optimal Trajectories Using Direct Transcription and Nonlinear Programming," *Journal of Guidance, Control, and Dynamics*, Vol. 15, No. 4, 1992, pp. 994–1002.

[9]Aston, G., "Ferry to the Moon," *Aerospace America*, Vol. 25, No. 6, 1987, pp. 30–32.

[10]Kluever, C. A., and Pierson, B. L., "Vehicle-and-Trajectory Optimization of Nuclear Electric Spacecraft for Lunar Missions," *Journal of Spacecraft and Rockets*, Vol. 32, No. 1, 1995, pp. 126–132.

[11]Kelley, J. H., and Yen, C. L., "Planetary Mission Opportunities with Nuclear Electric Propulsion," AIAA Paper 92-1560, March 1992.

[12]Jaffe, L. D., "Nuclear-Electric Reusable Orbital Transfer Vehicle," *Journal of Spacecraft and Rockets*, Vol. 25, No. 5, 1988, pp. 375–381.

[13]Hack, K. J., George, J. A., Riehl, J. P., and Gilland, J. H., "Evolutionary Use of Nuclear Electric Propulsion," AIAA Paper 90-3821, Sept. 1990.

[14]George, J. A., "Multimegawatt Nuclear Power Systems for Nuclear Electric Propulsion," AIAA Paper 91-3607, Sept. 1991.

[15]Szebehely, V. G., *Theory of Orbits, the Restricted Problem of Three Bodies*, Academic, New York, 1967, pp. 7–21.

[16]Egorov, V. A., *Three-Dimensional Lunar Trajectories*, Israel Program for Scientific Translations, Ltd., Jerusalem, Israel, 1969 (translated from the Russian).

[17]Anon., "User's Manual," Version 1.1, International Mathematics and Statistics Library, Houston, TX, Jan. 1989.

[18]Tang, S., and Conway, B. A., "Optimization of Low-Thrust Interplanetary Trajectories Using Collocation and Nonlinear Programming," *Journal of Guidance, Control, and Dynamics*, Vol. 18, No. 3, 1995, pp. 599–604.

[19]Pierson, B. L., "Sequential Quadratic Programming and Its Use in Optimal Control Model Comparisons," *Optimal Control Theory and Economic Analysis 3*, North-Holland, Amsterdam, 1988, pp. 175–193.

[20]Bryson, A. E., and Ho, Y. C., *Applied Optimal Control*, Hemisphere, New York, 1975, pp. 47–89.

[21]Herman, A. L., and Conway, B. A., "Direct Optimization Using Collocation Based on High-Order Gauss–Lobatto Quadrature Rules," *Journal of Guidance, Control, and Dynamics*, Vol. 19, No. 3, 1996, pp. 592–599.

[22]Edelbaum, T. N., "Propulsion Requirements for Controllable Satellites," *ARS Journal*, Vol. 31, No. 8, 1961, pp. 1079–1089.

[23]Dixon, L. C. W., and Biggs, M. C., "The Advantages of Adjoint-Control Transformations when Determining Optimal Trajectories by Pontryagin's Maximum Principle," *Aeronautical Journal*, March 1972, pp. 169–174.